Liver firewall function at the heart of mutualism between the host and its commensal intestinal microbes

Abstract:

A prerequisite for establishment of mutualism between the host and the dense microbial community that inhabits the lower large intestine is the stringent mucosal compartmentalization of microorganisms. Intestinal dendritic cells (DC) sample live microbes to induce mucosal immunity – microbe-loaded DC trafficking through lymphatics are arrested at the mesenteric lymph nodes (MLN), which constitute the firewall of the intestinal lymphatic circulation. We show that the liver, which receives the intestinal venous blood, is positioned as a vascular firewall if microbes enter the bloodstream in situations of intestinal pathology. The two firewalls act independently for lymphatic sampling and vascular translocation into intestinal venous blood respectively. Phagocytic Kupffer cells in the liver also clear commensals from the systemic vasculature independently of the spleen through the liver's own arterial supply. Damage to the liver firewall in mice impairs functional clearance of commensals from blood, despite heightened innate immunity, resulting in spontaneous priming of non-mucosal immune responses through increased systemic exposure to intestinal commensals. Systemic immune responses consistent with increased extraintestinal commensal exposure were also found in humans with liver disease (non-alcoholic steatohepatitis). Bacterial infections are the commonest cause of death in cirrhosis and the liver is a functional vascular firewall at the centre of host-microbial mutualism, required to clear commensals that penetrate either intestinal or systemic vascular circuits.

Introduction:

Liver disease is dramatically increasing in incidence in the developed world, secondary not only to alcohol abuse and viral infections but also to progressive hepatic fatty change and damage arising from a metabolic syndrome. All forms of chronic liver disease, including non-alcoholic fatty liver disease (NAFLD), potentially lead to cirrhosis and liver failure. Even with very mild liver disease, such as excess fatty accumulation in the liver, the structure of the sinusoids and Kupffer cell function are compromised (*1-3*). Cirrhosis imposes dramatically increased resistance to blood flow in the hepatic portal vein: the resulting increased pressure (portal hypertension) causes enlargement of the spleen, damage to the intestine and abnormal vascular channels (shunts) where the portal circulation bypasses the liver and drains directly into the inferior vena cava returning blood to the heart. Despite the fearsome metabolic complications of liver failure, the commonest cause of death in patients with terminal cirrhosis is from infections (*4*). Many of these infections are derived from oral or intestinal commensal organisms, resulting in peritonitis, spontaneous bacterial empyema or bacteraemia (*5*), so understanding the impact of liver function and dysfunction on host-microbial mutualism is highly relevant to human health.

Mesenteric lymph nodes are known to act as a firewall during the induction of mucosal immunity through the DC/lymphatic route in healthy mice with a normal intestinal mucosa (*6*). We have previously shown that live commensal bacteria are sampled by intestinal dendritic cells (DC), which can traffic to the mesenteric lymph nodes (*6, 7*). These intestinal DC normally do not penetrate further to reach systemic secondary lymphoid structures (*6*), thus induction of intestinal mucosal immune responses are compartmentalized to the intestinal mucosal immune system.

The liver receives both venous blood from the intestine via the hepatic portal vein, and arterial blood from the hepatic artery arising from the celiac trunk of the aorta. Although the liver is ideally positioned as a second firewall for commensals that succeed in reaching the mesenteric

or systemic vasculature, and dynamic studies have shown that its abundant Kupffer macrophage population can capture pathogens from the blood (*8, 9*), it has been unclear whether it has an obligatory role to limit penetration of commensal microbes that are sampled in the course of inducing normal mucosal immune responses. Here we show that the liver remains sterile when benign intestinal commensals are sampled through the lymphatic route in the healthy mouse intestine. However, the liver becomes important as an independent second firewall when commensal microbes penetrate the vasculature of the inflamed intestine or when commensal microbes have to be cleared from the systemic blood. In both animal models and human patients with liver disease, loss of this central firewall function progressively disrupts host microbial mutualism by increasing systemic exposure and systemic immune activation to intestinal commensals.

Results:

To determine whether the liver is also acting as a firewall during sampling of intestinal commensal bacteria in healthy wild-type mice we compared numbers of culturable bacteria in the mesenteric lymph nodes and the liver over time after gavaging germ-free mice with the reversible colonisation strain *E. coli* HA107 (*10*) or its parent strain JM83. In each case, live commensal bacteria penetrated to the mesenteric lymph nodes, from lymphatic trafficking of intestinal dendritic cells carrying commensals sampled at the intestinal epithelial surface (*6, 7*) (Fig. 1A). In contrast, the liver remained entirely sterile throughout the experiment (Fig. 1A). Similarly, (n=3) or in experiments designed to detect portal bacteraemia at earlier times live bacteria were never recovered from the portal blood in these mice (fig. S1A), suggesting that extremely efficient bacterial killing in the liver does not explain the lack of live bacterial recovery. Despite no penetration of live bacteria to the liver or induction of systemic immune responses (*6*, *10*) after intestinal challenge in healthy mice, we could demonstrate drainage of bacterial breakdown products to hepatic tissues after gavage of *E. coli* JS219 metabolically labelled during growth in the presence of [^{14}C]glucose (Fig. 1B). Therefore the penetration of live organisms to the mesenteric lymph nodes during induction of mucosal immunity can be uncoupled from penetration to either the liver or the spleen in a healthy animal, despite substantial accumulation of metabolites originating from intestinal bacteria in both organs. This suggests that in healthy animals, the liver is not a required part of the firewall that compartmentalises lymphatic-based mucosal immune induction, but rather functions for processing and detoxification of bacterial-derived material, or as a second firewall for those microbes that enter the mesenteric blood vessels as a result of increased epithelial penetration or during mucosal damage.

Venous blood from the intestine drains mainly to the liver via the hepatic portal vein, which is formed by the confluence of the superior mesenteric vein and the splenic/inferior mesenteric

vein (fig. S1B). To test the role of the liver as a firewall for the mesenteric vasculature, commensals were deliberately injected into the hepatic portal venous system: these were primarily cleared to the liver and to a minor extent to the spleen (Fig. 1C). As model commensal microbes do not penetrate to the liver when given as intestinal challenge doses to healthy pathogen-free mice, we next tested the effect of inducing intestinal inflammation. After treatment with dextran sodium sulphate (DSS), an intestinal dose of bacteria that would normally only penetrate within dendritic cells to the mesenteric lymph nodes, now consistently reached the liver (Fig. 1D) and in some animals could be detected in the spleen and peripheral blood (fig. S2A). We concluded that whilst the liver is not part of the firewall required to compartmentalize the mucosal lymphatics in healthy SPF mice, it is a vital vascular firewall for the mesenteric circulation, and likely critical to maintain mutualism in conditions of weakened mucosal-blood barrier function.

We next considered the role of the liver in clearing commensal microbes from the general systemic vasculature (not just the mesenteric/portal intestinal blood vessels). It is well documented that the spleen filters microorganisms within the general blood circulation: we have previously shown that live commensals given into the tail vein are cleared into the spleen, with only small numbers reaching the lymph nodes (*6*). However, splenectomy can be carried out in humans or experimental animals with relatively little disturbance in host-microbial mutualism provided there has been pre-immunization against encapsulated bacteria (*11*). The main vascular exchange structures of the liver – hepatic sinusoids – are a capillary level confluence of branches of the hepatic portal vein (which receives the splenic vein as a tributary) and the hepatic artery (fig. S1B) (*12*). This anatomical arrangement caused us to question whether the liver functions at the heart of host-commensal mutualism by clearing microbes within the general systemic vasculature through two possible routes: i) directly through filtration of blood from the hepatic artery, or ii) indirectly by filtering any overflow from the spleen or transit through

mesenteric vessels via the splenic→hepatic portal vein. Liver sinusoids are lined by enormous numbers of Kupffer cell phagocytes, which constitute over 80% of all tissue macrophages in the body and about 20% of all hepatic cells and which are present in normal numbers in germ-free animals (*13*, *14*). These are capable of taking up and killing microorganisms that they encounter (*8, 9, 15*, *16*). Indeed, we found that doses of commensals given intravenously caused culturable commensals to be detected in the liver of wild-type mice, and this effect was not significantly different in splenectomised mice (Fig. 1E), verifying an effective systemic vascular clearance to the liver, independently of the spleen, probably mostly through the hepatic blood supply. We then examined the role of the hepatic arterial supply in delivering commensals to the liver in animals where the spleen is present. After ligating the hepatic artery (a non-essential vascular supply of the liver) prior to administering the venous dose of commensals clearance to the liver was significantly reduced compared with sham-operated animals in which the artery was exposed but not ligated (Fig. 1F) and clearance from the blood was also delayed (3 hours: ligated 203 ± 69 CFU/50 µl versus sham 41 ± 26 CFU/50 µl, mean ± SD, n=5). The liver therefore forms a critical part of the filtration system that clears systemic commensal bacteraemia through both the arterial and portal venous circuits.

To address the function of the liver in clearing, as opposed to merely capturing commensals that have reached the systemic circulation, we carried out trajectory experiments to measure the presence of commensals in the peripheral general circulation over time following an experimental intravenous dose. We started by asking whether depletion of Kupffer cells in the liver would impair the clearance of commensals from the general vasculature independently of the spleen. To do this, clodronate liposomes were injected into C57BL/6 mice to deplete phagocyte populations, after prior splenectomy (*17*). Even in the absence of the spleen, clodronate treatment resulted in delayed clearance of bacteremia from a challenge dose of *E. coli* K-12 (Fig. 2A, fig. S2B) given three days later into the tail vein. Although there is probably a

small effect of macrophages outside the liver, hepatic Kupffer cells form the majority of body macrophages and culture experiments showed that >86% of culturable model commensal bacteria were recovered from either the liver or spleen following intravenous challenge in wild-type unmanipulated animals. Given that there is also delayed clearance of commensals from the peripheral general vasculature in the setting of liver disease (Fig. 2B, fig. S3A-C) and that mice with liver disease show increased liver bacterial burdens after intravenous bacterial challenge (fig. S3D), we concluded that bacterial clearance by Kupffer cells in the liver is an important mechanism for the removal of live commensals from the blood, mirroring their role in dynamic studies of pathogen clearance.

To examine the effects of liver dysfunction on host microbial mutualism specifically, we studied two independent models of liver disease. First, we measured the trajectory of clearance of challenge doses of *E. coli* K-12 in cirrhotic mice following bile duct ligation (BDL) compared with sham-operated controls. This showed significantly reduced efficiency of clearance of commensal bacteria from the blood and spleen of cirrhotic mice (Fig. 2, B and C). This was observed despite a dramatic increase in the number of blood granulocytes in the circulation of BDL mice (fig. S4A) and evidence of stronger release of acute phase proteins (Lipocalin2) into the serum (fig. S4B). Therefore, despite heightened inflammatory responses to challenge, liver disease was associated with a strong reduction in bacterial clearance ability of the mice. As bile-duct ligation in mice induces cholestasis and thus altered bile salt recycling and some degree of intestinal pathology, we used an additional model of liver disease that allowed us to study the trajectory of host microbiota mutualism in liver disease. Clearance of an intravenous challenge dose of bacteria from the blood, liver and spleen was also delayed if the liver was damaged using carbon tetrachloride (CCl_4) treatment (causing less severe hepatic fibrosis at early stages) (*18*) (Fig. 2D, fig. S3 and S5). Importantly, CCL_4 treated mice showed normal distribution of liver Kupffer cells on histological specimens supporting the concept of altered phagocytic capacity

rather than simply disrupted liver architecture, reduced numbers of immune cells and fibrotic replacement in liver disease (fig. S5D).

We speculated whether this altered bacterial clearance ability during murine liver disease could be due to “exhaustion” of the innate immune system by accumulated bacterial products in the systemic circulation. To investigate this possibility, we serially pretreated mice with increasing doses of *Salmonella*-LPS over 21 days (to match the timing of bacterial challenge in BDL mice after surgery). However, when these preconditioned mice were challenged with an intravenous dose of a non-pathogenic *E. coli* they displayed greatly enhanced bacterial clearance compared to control animals, despite non-cross-reactivity between the LPS used for pre-treatment and that of the challenge strain (Fig. 2, E and F, fig. S6, A and B). An expansion of blood granulocytes was also observed in LPS-conditioned mice (data not shown). Therefore increased exposure to microbial products alone was insufficient to cause the observed commensal clearance defects, in the absence of liver disease. We also considered whether the integrity of the mesenteric lymph node firewall was impaired in the setting of liver disease. We verified that an intestinal challenge dose of *E. coli* reached the mesenteric lymph nodes equivalently whether or not there was hepatocellular damage in the CCl_4 model, but there was no further penetration to the thoracic duct lymph, showing that the mesenteric firewall remained intact (fig. S6C). These defects of clearance of commensal bacteria from the systemic circulation could be detected in acute CCl_4 liver disease in mice colonized with a strict altered Schaedler flora (ASF; a very simple benign microbiota consisting of 8 microbial species) and with no evidence for dysbiosis or defects in mesenteric lymph node barrier function or intestinal integrity (fig S6C and S7A). More advanced liver disease (such as observed in BDL) certainly causes secondary histological damage to the intestine (fig. S7B) as well as low-grade intestinal inflammation measured through the fecal content of the neutrophil activation marker lipocalin-2 (fig. S7C) as a result of the effects of increased pressure in the portal circulation. Therefore in the face of advancing liver

disease, there is a combination of increased probability of intestinal microbes translocating into the vasculature and decreased ability to clear these microbes from portal or systemic blood.

To follow the functional consequences of liver dysfunction on host-microbial immune mutualism in both mouse and human we needed to interrogate low levels of systemic exposure to intestinal commensal microbes independently of intestinal or systemic challenge doses in both murine models of liver disease and in human patients. To do this, we made use of immunoglobulin isotype differences that occur when commensal bacteria induce immune responses in different body compartments (*19*). We have previously demonstrated that the response to commensals typically found in SPF mice is compartmentalised to the mucosa and hence to mucosal IgA (*6, 19*). Serum IgG against commensals can be experimentally induced by deliberate injection of commensal organisms into the tail vein, but is absent from specific-pathogen free (SPF) wild-type mice (*19*). Anti-commensal serum IgG also occurs spontaneously in mice that inefficiently clear commensals (defective Toll-like receptor signalling resulting from MyD88/TRIF adaptor deficiency or in mice deficient in the enzyme pathways required to generate oxygen or nitric oxide radicals for biocidal activity in phagocytes), as live commensals can then reach and induce immunity in systemic secondary lymphoid structures (*20*). Therefore, the presence of high titres of specific serum IgG directed against commensal microbes can be used as a surrogate marker of commensal penetration to the systemic immune system.

To validate the concept of examining induction of specific serum IgG against dominant intestinal commensals, we used a trajectory of exposure to CCl_4 as a sequential progressive model of liver disease. In early liver disease, specific serum IgG against commensals of the microbiota were absent, but these appeared as the liver disease progressed, measured using a specific FACS-based assay which assesses specific surface Ig binding to the endogenous microbes (*20*), normalised for total IgG concentration (Fig. 3, A to F). Specific serum IgG against commensal

microbes, such as autologous *Lactobacillus sp*. or bulk cultured aerobes was also increased in mice or rats with a more diverse microbiota that had developed fibrosis following bile duct ligation (Fig. 3, E and F, fig. S8).

A critical issue in modelling human disease is that rodent models of cirrhosis develop over weeks and months, compared with human disease that can develop over decades. The question was whether early liver disease in humans (with its associated microvascular and phagocytic abnormalities (*1, 3*)) is associated with abnormalities of handling and compartmentalising intestinal commensals, or whether disturbance of host-microbial mutualism only develops with very advanced liver pathology. To address this we assembled two separate cohorts of patients, from different University Hospitals in Italy and Switzerland. In the first cohort, we compared patients with non-alcoholic fatty liver disease and matched control patients. In the second we were able to examine patients with liver steatosis, non-alcoholic steatohepatitis (NASH) and cirrhosis compared with controls. In most cases of liver steatosis or NASH the patient has no symptoms of the disease and there is no metabolic liver failure, although some cases will later progress to cirrhosis. Strikingly, in both cohorts, these early cases of human liver disease also had evidence of increased serum IgG and IgA responses against both aerobic and anaerobic non-pathogenic intestinal commensals independently of the stage of disease (Fig. 4A and S9A) and Euclidean heatmaps of the responses were also discriminatory for diagnosis in unbiased cluster analysis (Fig. 4B and S9B). This suggests that impaired liver phagocyte capture of bacteria is a likely contributor to human liver disease that exacerbates other features of the underlying etiology.

As early stages of disease are not associated with porto-systemic vascular shunting or drastic metabolic failure of the liver, we concluded that disrupted host-microbiota mutualism is amongst the earliest consequences of human liver disease.

Discussion:

We have found that compartmentalisation of commensal intestinal microbes is defective in animal models of liver disease. Interestingly, this was not due to loss of function in the well-described primary lymphatic firewall that functions during normal mucosal sampling of intestinal bacteria, but due to failure of a hepatic vascular firewall that is required to clear blood-borne commensals from the mesenteric and systemic vasculature efficiently. Disturbed compartmentalization during murine liver dysfunction resulted in spontaneously increased systemic immune responses to resident commensals without intestinal challenge or overt intestinal pathology. This is consistent with bacterial exposure of the systemic lymphoid structures secondary to increased penetration and reduced commensal clearance from the vasculature despite increased innate immune activity. As murine and human liver disease is associated with increased complement activity (*21*), impaired liver bactericidal capacity is likely to be a major contributor to increased systemic commensal bacterial exposure in liver disease. In human patients, similar systemic immune responses to commensals are observed very early in the course of the human condition long before cirrhosis has developed. Even though it was not possible to collect patient fecal samples in order to normalize to each patient's microbiota composition, we found systemic immune responses against a selection of non-pathogenic commensal bacteria to be discriminatory for diagnosis in unbiased cluster analysis. It is known that dysbiosis of intestinal microbes can precede and trigger liver damage (*22, 23*): this is also likely to be an initiating event in at least some human patients, although it is not required *per se* for the disturbance in host microbial mutualism as in our mouse model the very simple ASF microbiota was tightly controlled and liver damage was provoked by other methods. Thus we were able to separate dysbiosis from the direct effects of liver disease on systemic bacterial handling. This revealed a critical requirement for liver ultrastructure and function to clear bacteria. Our observations in human liver disease highlight that such mechanisms are essential to maintain normal host-microbiota homeostasis in the context of frequent "real-world" challenges

to intestinal integrity. It is possible that monitoring anti-microbiota IgA and IgG titres in liver patients may identify those with the highest risk of infectious complications and may thus have diagnostic value. Failed compartmentalization and vascular clearance of commensals are likely to be important factors resulting in catastrophic infective complications of patients with end-stage liver disease such as spontaneous bacterial peritonitis and sepsis which is predominantly caused by organisms of intestinal origin.

Materials and Methods:

Animal experiments. *Liver fibrosis models:* For analysis of serum anti-microbiota antibodies, BDL treatments were performed at Ghent University Hospital, Belgium in C57BL/10 mice as described previously (*24*). Briefly, a midline abdominal incision was made and the common bile duct was isolated and occluded with a double ligature of a non-resorbable suture. The first ligature was made below the junction of the hepatic ducts and the second was made above the entrance of the pancreatic duct. The common bile duct was sectioned between the two ligatures and mice were euthanized 6 weeks after BDL. In sham-operated mice, ligatures were placed identically but no section was made. CCl_4 was administered intra-peritoneally in C57BL/6 mice colonised with an Altered Schaedler flora consisting of 8 bacterial species (*Actobacillus acidophilus* (strain ASF 360), *Lactobacillus salivarius* (strain ASF 361), *Bacteroides distasonis* (strain ASF 519), *Flexistipes sp*. (ASF 457), *Clostridium* cluster XIV group (ASF 356, ASF 492, ASF 500 and ASF 502)) twice weekly (1:4 dissolved in olive oil; 60 µl per animal), whereas control animals received 60 µl olive oil. Mice were analysed after 6, 12 and 16 weeks.

For bacterial clearance measurements, A. DeGottardi performed BDL treatments in gnotobiotic NMRI mice in Bern, as described above. Mice were analysed 3 weeks after surgery.

Rat bile-duct ligation was performed as described previously (*25*). 7 weeks old male Wistar rats (Charles River) were housed in IVC cages at the University Bern.

LPS pre-conditioning experiments: Swiss Webster mice housed under ultraclean conditions at the ETH Zürich department of microbiology were treated 3 times per week with PBS alone or with 1 µg LPS from *Salmonella* Typhimurium intraperitoneally and analysed 48h after the final treatment.

DSS-colitis induction: 14 weeks old SPF C57BL/6 mice were treated with 3 cycles of DSS (molecular weight 36’000 – 50’000, MP) in drinking water for 5 days (Week 1: 1% DSS, week 2: 1.5% DSS, week 3: 2% DSS) followed by 4 days of normal drinking water. All mice were

anaesthetised with CO_2 prior to terminal bleeding, and livers were aseptically removed for bacterial analysis.

Hepatic artery ligations: After midline abdominal incision the hepatic artery was prepared and 2 ligatures placed, followed by section of the hepatic artery. In sham-operated animals, the hepatic artery was only exposed and ligatures placed but not sectioned. *Splenectomies*: Splenectomy was performed in 8-10 weeks old mice. After midline abdominal incision, the spleen was exposed and splenic artery and vein ligated before removal of the spleen and suture of the peritoneum and skin.

Intra-mesenteric vein bacterial challenge: After midline abdominal incision, 10^7 *E. coli* JM83 or PBS in a volume of 100 µl were injected into the mesenteric veins of 8-10 weeks old mice with an insulin syringe followed by compression of the vessel for 2 minutes to stop bleeding. The peritoneum and skin were then closed with a suture. Animals were euthanized 8 hours after challenge and organs aseptically removed for plating and counting of CFUs.

Preparation of clodronate liposomes: Clodronate liposomes were generated as described previously (*17*) and the effectiveness of depletion was validated by FACS. Briefly, a dry lipid mixture was solubilised with clodronate (Ostac, Boehringer, Mannheim) and the resulting multilammelar vesicles were filter-extruded. Unencapsulated clodronate was then removed by ultrafiltration followed by size exclusion chromatography. Liposomes were then re-concentrated (3-5 mg/ml) and sterile-filtered. C57BL/6 mice were i.v.-injected with liposomes containing 2-2.5 mg clodronate 3 weeks after splenectomy and challenged with live *E. coli* K-12 into the tail vein 3 days later to determine bacterial clearance capacity.

Peripheral blood granulocyte numbers: Determination of granulocyte counts/microliter was performed using a VetABC animal blood counter (Medical Solution GmbH).

From all animal models, fresh faecal pellets and serum were collected and used immediately or stored at -80°C prior to use.

All animal experiments were approved by the local Animal Care Committee.

***Colonisation with ^{14}C labelled E. coli* K-12.** Germ-free C57BL/6 mice were monocolonized with ^{14}C-labeled *E. coli* JS219 and liver biopsies were taken at 7, 24, 48 and 126 after colonization for culture on LB agar and to measure levels of radioactivity. Samples for radioactivity were dissolved in 1 ml of NCS II Tissue solubilizer (GE Healthcare) for a minimum of one hour at 56°C, at which time the pH level was neutralized with 100 μl of 100% glacial acetic acid and the sample was mixed with 18 ml of ULTIMA Gold™ liquid scintillation cocktail (PerkinElmer) prior to measuring radioactivity. ^{14}C radioactivity levels in each sample were counted in a TRI-Carb 2300TR Liquid Scintillation Anaylzer (Packard) for a maximum time of 5 minutes. Colorimetric quench curves were used to ensure accurate measuring of samples. Background levels of radioactivity were determined by measuring the levels of ^{14}C in mesenteric lymph nodes and livers of germ-free C57BL/6 mice (n=2).

E. coli HA107/JM83 mono-colonisation. Colonisation was performed as described previously (*10*). Briefly, D-Ala (200 μg/ml)/*m*-DAP (50 μg/ml)-supplemented LB cultures were aseptically inoculated from single colonies of *E. coli* strains HA107 or JM83 and incubated with shaking at 160 rpm at 37°C for 18 hours. Bacteria were harvested under axenic conditions by centrifugation (15 min, 3500X g, 4°C), washed in sterile PBS and concentrated to a density of 2×10^{10} CFU/ml in PBS. The bacterial suspensions were sealed in sterile tubes and imported into flexible film isolators, where 500 μl (10^{10} CFU) were gavaged into the stomachs of germ-free Swiss Webster mice. Faecal samples exported from the isolator were bacteriologically analysed to monitor *E. coli* shedding and microbiological status of the inoculated mice. The same protocol was used to prepare bacteria for intra-venous injections.

Bacteriology. Animals were euthanized and livers, spleens and mesenteric lymph nodes removed aseptically. For sampling of thoracic duct lymph, animals were gavaged with olive oil 2 hours before analysis. The thoracic duct was then exposed and lymph sampled with a sterile micro-capillary for plating on agar plates. Organs were homogenised in 0.5% Tergitol/PBS using a Tissuelyser (Retsch MM400, 25Hz) and sterile stainless-steel ball bearing beads and

homogenates plated on supplemented agar plates for overnight culture at 37°C and CFU quantification.

Isolation of faecal bacteria. Fresh faecal pellets were dissolved in 1 ml sterile PBS and streaked out onto LB and Blood agar plates. Plates were then incubated aerobically (LB) and anaerobically (Blood agar) for 24 or 48-72 hours respectively. Single colonies were grown in liquid brain-heart infusion medium (Oxoid, #CM0225) and used for bacterial FACS and 16S PCR to identify the bacterial species.

16S rRNA Sequencing. 1 ml of a 5 ml overnight culture was pelleted by centrifugation at 7000 rpm for 3 minutes Pellets were then dissolved in 250 µl direct PCR lysis reagent (Viagen Biotech Inc., # [102-T]) containing 5 µl proteinase K (Roche, # 3115887001). Samples were then incubated for 1 hour at 55°C followed by 1 hour at 85°C to inactivate proteinase K. 5 µl DNA template was then used for PCR, using 1 µl forward 10µM primer FD1 (AGA GTT TGA TCC TGG CTC AG), 1 µl forward 10µM primer FD2 (AGA GTT TGA TCA TGG CTC AG), 1 µl reverse 10 µM primer RP1 (CG GTT ACC TTG TTA CGA CTT), 1µl dNTP (Promega, #U1515), 0.4 µl Taq polymerase (Promega, #M3175), 10 µl 5x buffer and 30.6 µl molecular water per reaction. PCR was performed according to the following set-up: 94°C 5 minutes 94°C 1 min, 43°C 1 min, 72°C 2 min – repeat 35x, 72°C 7 min, 10°C forever. PCR purification was then performed using the MiniPrep kit (Qiagen, #28004) and DNA eluted in 10 µl water. DNA concentration was measured with a Nanodrop ND-1000 (Thermo Scientific) and 1 µl DNA plus 1 µl FD1 primer in 18 µl molecular water was sent for 16S sequencing (Microsynth).

NAFLD cohorts and controls. Serum samples from 2 different patient cohorts of NAFLD were collected in accordance with local ethical committees. The Basel cohort consisted of 28 patients with elevated aminotransferase levels and drinking less than 40 g (males) or 20 g (females) alcohol/week with biopsy-proven NAFLD (age (mean ± SD): 49 ± 16 years, sex (m/f): 18/10) and the Rome cohort consisted of 16 patients with biopsy-proven NASH drinking less than 20 g alcohol/day (age (mean ± SD): 50 ± 13 years, sex (m/f): 2/14) (*26*). All patients had biopsy-

proven NAFLD and alcohol intake was assessed by patient history. For Rome patients also one close relative was interviewed and an AUDIT test was performed and had to be less than 7 (*27*). Patients from the Basel cohort were further divided into a steatosis, NASH and cirrhosis group on the basis of the NAFLD activity score (NAS (*28*)). Frozen serum samples were stored at -80°C prior to analysis. Healthy control samples were obtained from individuals interviewed to exclude acute illness or prior liver or intestinal disease. A selection of 4-16 precisely age- and sex-matched controls was used for each patient cohort. All experiments were performed in accordance with the local ethical committee approval and guidelines.

ELISAs. Total concentrations of antibody isotypes in mouse or human serum were determined by sandwich ELISA. Mice: Coating antibodies were goat-anti-mouse IgG1, 2b, A and M (Serotech) and detection antibodies were HRP-conjugated anti-mouse IgG, IgM or IgA (Sigma). Standards were myeloma-derived purified IgG1, IgG2b, IgM (Invitrogen) and IgA (BD Pharmingen). Humans: IgG and IgA antibodies were determined using the Human IgG and IgA ELISA Quantitation Kit (Lubio Science, #E80-104, #E80-102).

Bacterial FACS analysis. Bacterial FACS analysis was performed as described previously (*10, 20*). Briefly, 5 ml LB cultures were inoculated from single colonies of plated bacteria and cultured overnight at 37°C without shaking. 1 ml of culture was gently pelleted for 3 mins at 7000 rpm in an Eppendorf minifuge and washed 3x with sterile-filtered PBS/2%BSA/Azide before re-suspending at approximately 10^7 bacteria per ml. Mouse or human serum was diluted 1:10 in PBS/2%BSA/Azide and heat-inactivated at 60°C for 30 minutes. The serum solution was then spun at 13000 rpm in an Eppendorf minifuge for 10 minutes to remove any bacteria-sized contaminants and the supernatant was used to perform serial dilutions. 25 µl serum solution and 25 µl bacterial suspension were then mixed and incubated at 4°C for 1 h. Bacteria were washed twice before re-suspending in monoclonal FITC-anti-mouse IgG2b or IgA, PE-anti-mouse IgG1 and APC-anti-mouse IgM (BD Pharmingen, #559354, #550083, #553395, #550676) or Dyelight647-anti-human IgG, FITC-anti-human IgA (Jackson Immunoresearch). After a further

hour of incubation the bacteria were washed once with PBS/2% BSA/Azide and then re-suspended in 2% PFA/PBS for acquisition on FACSArray using FSc and SSc parameters in logarithmic mode. Data were analysed using FlowJo software (Treestar, USA) and titres calculated by fitting 4-parameter logistic curves to each donor and determining the concentration of IgG or IgA required to give a median fluorescence intensity binding significantly above background. The inverse of this IgG or IgA concentration is shown, for ease of interpretation.

Heatmap analysis. Heatmaps and correlation analysis was performed using R-software (http://www.r-project.org/). Heatmaps were generated for scaled, normalized titre data using an euclidean distance function with complete linkage clustering in R using the package "gplots version 2.8.0", function "heatmap.2".

Serum lipocalin 2 ELISA. Lipocalin 2 values, as a marker of granulocyte activation and an acute phase-response, were determined by ELISA according to the manufacturer's instructions with a few modifications (human: R&D systems, #DY1757, murine: R&D systems, #DY1857). Nunc Immuno Plates C96 Maxisorp (Milian, #430341) were coated with 50 µl capture antibody (1:200 in PBS) overnight at 4°C in a humidified chamber. After washing in PBS/Tween0.05% (Sigma, # P2287-500ML) and blocking in 150 µl PBS/BSA1% for 15 minutes at RT, samples and standard were added in 3-fold dose-titrations starting at 1:10 (serum and standard) or neat (faecal pellets, re-suspended in 1 ml PBS) and incubated overnight at 4°C in a humidified chamber. After washing in PBS/Tween0.05%, 50 µl detection antibody (1:200 in PBS/BSA2%) was added and plates incubated for 1 hour at RT. Plates were then washed in PBS/Tween0.05% and 100 µl HRP-Streptavidin (Biolegend, # 405210 1:1000 in PBS) was added for 1 hour. Plates were then washed and developed with 100 µl substrate (10 ml substrate buffer, 1 mg ABTS, 10 µl H_2O_2). OD was measured at 415nm and four-parameter curves generated to compare EC50 values of samples and standards.

Histological analysis. Intestinal tissue samples were embedded in OCT, snap-frozen in liquid nitrogen, and stored at –80°C. Cryosections (5 µm) were mounted on glass slides, air dried for 2

h at room temperature, and stained with hematoxylin and eosin (H&E). Livers were fixed in 4% formaldehyde for 24 hours followed by ethanol 70% for 48 hours. Samples were then paraffin embedded, cut, and stained with H&E, F4/80 or Masson's Trichrome respectively.

Statistical analysis. Differences were analysed for statistical significance using Prism 4 for Macintosh (GraphPad software Inc). The details of the test carried out are indicated in figure legends. Where data was approximately normally distributed, values were compared using either a student t-test for single variable, or 2-way ANOVA for two variables. Approximate P values were computed for 2-way ANOVA. Where data were not normally distributed, (e.g. including bacterial CFU counts close to or equal to zero) non-parametric 2-tailed Mann-Whitney U tests were applied. In all cases, $p < 0.05$ was considered significant.

References:

1. S. Ijaz, W. Yang, M. C. Winslet, A. M. Seifalian, Impairment of hepatic microcirculation in fatty liver. *Microcirculation (New York, N.Y. : 1994)* 10, 447 (Dec, 2003).
2. B. Vollmar, S. Siegmund, M. D. Menger, An intravital fluorescence microscopic study of hepatic microvascular and cellular derangements in developing cirrhosis in rats. *Hepatology* 27, 1544 (Jun, 1998).
3. T. Asanuma *et al.*, Super paramagnetic iron oxide MRI shows defective Kupffer cell uptake function in non-alcoholic fatty liver disease. *Gut* 59, 258 (Feb, 2010).
4. V. Arvaniti *et al.*, Infections in patients with cirrhosis increase mortality four-fold and should be used in determining prognosis. *Gastroenterology* 139, 1246 (Oct, 2010).
5. T. Gustot, F. Durand, D. Lebrec, J.-L. Vincent, R. Moreau, Severe sepsis in cirrhosis. *Hepatology (Baltimore, Md)* 50, 2022 (Dec, 2009).
6. A. J. Macpherson, T. Uhr, Induction of protective IgA by intestinal dendritic cells carrying commensal bacteria. *Science (New York, NY)* 303, 1662 (Apr 12, 2004).
7. M. Rescigno *et al.*, Dendritic cells express tight junction proteins and penetrate gut epithelial monolayers to sample bacteria. *Nat Immunol* 2, 361 (Apr, 2001).
8. J. G. Egen *et al.*, Macrophage and T cell dynamics during the development and disintegration of mycobacterial granulomas. *Immunity* 28, 271 (Mar, 2008).
9. W.-Y. Lee *et al.*, An intravascular immune response to Borrelia burgdorferi involves Kupffer cells and iNKT cells. *Nature immunology* 11, 295 (May, 2010).
10. S. Hapfelmeier *et al.*, Reversible microbial colonization of germ-free mice reveals the dynamics of IgA immune responses. *Science (New York, NY)* 328, 1705 (Jul 25, 2010).
11. A. Di Sabatino, R. Carsetti, G. R. Corazza, Post-splenectomy and hyposplenic states. *Lancet* 378, 86 (Jul 2, 2011).
12. B. Smedsrød *et al.*, Cell biology of liver endothelial and Kupffer cells. *Gut* 35, 1509 (Nov, 1994).
13. L. Bouwens, M. Baekeland, R. De Zanger, E. Wisse, Quantitation, tissue distribution and proliferation kinetics of Kupffer cells in normal rat liver. *Hepatology* 6, 718 (Jul-Aug, 1986).
14. D. L. Knook, C. Barkway, E. C. Sleyster, Lysosomal enzyme content of Kupffer and endothelial liver cells isolated from germfree and clean conventional rats. *Infection and immunity* 33, 620 (Aug, 1981).
15. G. Baffy, Kupffer cells in non-alcoholic fatty liver disease: the emerging view. *J Hepatol* 51, 212 (Jul, 2009).

16. G. J. Thorbecke, B. Benacerraf, Some histological and functional aspects of lymphoid tissue in germfree animals. II. Studies on phagocytosis in vivo. *Annals of the New York Academy of Sciences* 78, 247 (Jun 08, 1959).
17. P. Seiler *et al.*, Crucial role of marginal zone macrophages and marginal zone metallophils in the clearance of lymphocytic choriomeningitis virus infection. *European Journal of Immunology* 27, 2626 (Oct, 1997).
18. D. E. Fouts, M. Torralba, K. E. Nelson, D. A. Brenner, B. Schnabl, Bacterial translocation and changes in the intestinal microbiome in mouse models of liver disease. *Journal of hepatology* 56, 1283 (Jul, 2012).
19. A. J. Macpherson *et al.*, A primitive T cell-independent mechanism of intestinal mucosal IgA responses to commensal bacteria. *Science (New York, N.Y.)* 288, 2222 (Jul 23, 2000).
20. E. Slack *et al.*, Innate and adaptive immunity cooperate flexibly to maintain host-microbiota mutualism. *Science (New York, NY)* 325, 617 (Jul 31, 2009).
21. S. Hillebrandt *et al.*, Complement factor 5 is a quantitative trait gene that modifies liver fibrogenesis in mice and humans. *Nature genetics* 37, 835 (Aug, 2005).
22. M. Vijay-Kumar *et al.*, Metabolic syndrome and altered gut microbiota in mice lacking Toll-like receptor 5. *Science (New York, NY)* 328, 228 (May 09, 2010).
23. J. Henao-Mejia *et al.*, Inflammasome-mediated dysbiosis regulates progression of NAFLD and obesity. *Nature*, (Mar 01, 2012).
24. B. Blomme *et al.*, Alterations of serum protein N-glycosylation in two mouse models of chronic liver disease are hepatocyte and not B cell driven. *American journal of physiology Gastrointestinal and liver physiology* 300, G833 (Jun, 2011).
25. S. S. Lee, C. Girod, A. Braillon, A. Hadengue, D. Lebrec, Hemodynamic characterization of chronic bile duct-ligated rats: effect of pentobarbital sodium. *The American journal of physiology* 251, G176 (Aug, 1986).
26. L. Miele *et al.*, Increased intestinal permeability and tight junction alterations in nonalcoholic fatty liver disease. *Hepatology (Baltimore, Md)* 49, 1877 (Jul 01, 2009).
27. J. B. Saunders, O. G. Aasland, T. F. Babor, J. R. de la Fuente, M. Grant, Development of the Alcohol Use Disorders Identification Test (AUDIT): WHO Collaborative Project on Early Detection of Persons with Harmful Alcohol Consumption--II. *Addiction (Abingdon, England)* 88, 791 (Jul, 1993).
28. D. E. Kleiner *et al.*, Design and validation of a histological scoring system for nonalcoholic fatty liver disease. *Hepatology (Baltimore, Md)* 41, 1313 (Jul, 2005).

Acknowledgements:

We thank J. Kirundi, S. Rupp, J. Cahenzli, B. Flogerzi, C. Furer, H. Sägesser, J. Reichen and L. Idrissova for technical support, Reto A. Schwendener for generation of the clodronate liposomes and R. Blumberg, R. Germain, M. R. Thursz, C. Müller and R. Wiest for helpful comments. Grant support: Swiss National Science Foundation (310030-124732, 313600-123736 to A.J.M), Canadian Institutes of Health Research and the Genaxen Foundation. M.L.B. was supported by the Swiss Cancer League and the Swiss National Foundation (Grant 313600-123736/1). S.H. and K.D.M. are supported by a European Research Council Starting Grant. N.D. was supported by the Swiss National Foundation (Grant 138392). The authors have no conflicts of interests to declare.

Figure Legends:

Fig. 1. Firewall function of the liver in host-microbial mutualism. (**A**) Bacterial counts per gram of organ (liver = triangles, mesenteric lymph nodes = dots) is shown at the indicated time-points after oral gavage of NMRI mice with 10^{10} *E. coli* K-12 JM83 (filled symbols) and reversible colonizing *E. coli* HA107 (open symbols). (**B**) Bacterial products and live bacteria in the mesenteric lymph nodes (dots) and liver (triangles) after monocolonisation of germ-free C57BL/6 mice with ^{14}C-labelled *E. coli* JS219 at the indicated time-points after gavage. Radioactiave counts as a measure of bacterial products in liver and MLNs are shown as DPM on the left y-axis (open dots and triangles) and live bacteria are shown as CFU/g tissue on the right y-axis (filled symbols). (**C**) Bacterial counts in the liver (triangles) and spleen (dots) 8 hours after intra mesenteric vein injection of PBS (open symbols) or 10^4 *E. coli* JM83. (**D**) Liver colony-forming units in 14-weeks old C57BL/6 mice after a DSS treatment regimen of 1%, 1.5% and 2% DSS in drinking water for 5 days each, followed by a normal water interval of 4 days each. Control mice received normal water throughout the experiment. Livers were then aseptically removed after the last drinking water period and CFUs assessed after anaerobic and aerobic culture on blood agar or LB plates respectively. Shown are the pooled counts from both types of plates. (**E**) Bacterial counts in the liver of splenectomised (squares) or sham-operated mice (dots) 18 hours after intra-venous injection of 10^7 *E. coli* JM83 (filled symbols) or PBS (open symbols) into the tail vein. (**F**) Bacterial counts per liver in C57BL/6 mice 48 hours after ligation of the hepatic artery (open circles) or sham operation (filled dots). All mice were intravenously challenged with 10^7 *E. coli* K-12 and killed after 18 hours for plating of livers and spleens. All mice were 8-10 weeks of age, each data point represents a single animal from one experiment and horizontal lines show means. The dashed lines show the detection limit. Unpaired t-test was used to compare the groups.

Fig. 2. Liver firewall function is compromised in liver disease independently of alterations in innate immunity. (**A**) Bacterial counts in peripheral blood at the indicated time-points after intra-venous injection of 10^7 live *E. coli* into the tail vein of splenectoized and Kupffer-cell depleted (Clodronate, filled dots, solid line) or healthy control mice (open circles, dashed line). Kupffer cells were depleted 3 weeks after splenectomy in C57BL/6 mice by injecting clodronate liposomes 3 days prior to live bacterial challenge. Joining lines connect the means of each group. The horizontal dashed line represents the detection-limit. (**B**) Bacterial counts in peripheral blood at the indicated time-points after intra-venous injection of 10^7 live *E. coli* into the tail vein of bile-duct ligated (BDL, filled dots, solid lines) or sham-operated mice (open circles, dashed lines), 3-weeks after surgery. Shown are pooled data from two independent experiments. Joining lines connect the means of each group. The horizontal dashed line represents the detection-limit. (**C**) Bacterial counts per spleen of the same mice as in B, 6 hours after live bacterial challenge. Horizontal lines show means. (**D**) Bacterial counts in the spleen of CCl_4 treated (black dots) or healthy control mice (open circles) 6 hours after live bacterial challenge with 10^7 *E. coli* into the tail vein. C57BL/6 mice were intra-peritoneally injected two times per week with CCl_4 or olive oil respectively for 16 weeks. Horizontal lines show means. (**E, F**) Bacterial counts in peripheral blood (E) and spleen (F) in PBS or LPS injected mice 3 hours after injection of 10^7 live *E. coli* into the tail vein. All mice were treated 3 times per week with PBS alone or with 1 µg LPS from *Salmonella typhimurium* intraperitoneally and analysed 48h after the final treatment. All mice were then intravenously injected with 10^7 live *E. coli.* Bacterial counts were determined per 50 µl blood or organ. All mice were 8-10 weeks of age, each data point represents a single animal from one experiment and horizontal lines show means. Unpaired t-test was used to compare the groups.

Fig. 3. Increased systemic immune priming by intestinal commensal microbes in animal models with liver dysfunction. (**A-D**) Serum IgG1 (A, C) or IgG2b (B, D) titers against bacteria isolated from the mice's own faeces (*Clostridium sp*.) in healthy control (black dots) and fibrotic C57BL/10 mice as determined by bacterial FACS. Liver fibrosis was induced by a 6 (A and B) or 12 (C and D) weeks treatment with CCl_4, intra-peritoneally administered two times per week or olive oil as control. **(E, F)** Serum IgG1 (E) and IgG2b (F) titers of the mice shown in A-D. IgG-titers were calculated by fitting 4-parameter logistic curves to each sample and determining the concentration of IgG required to give a median fluorescence intensity binding above background staining. The inverse of this IgG concentration is shown, for ease of interpretation. Unpaired t-test was used to compare the groups. (**G**) Serum IgG1 titers against an autologous commensal bacterium (*Lactobacillus murinus*) isolated from the faeces in bile-duct ligated (BDL, open circles) or sham-operated control mice (black dots) 21 days after surgery. (**H**) Serum IgG-titers against an anaerobic bulk culture inoculated from the animals faeces 28 days after bile-duct ligation (filled dots) or sham-surgery (open circles) in rats. A-H Dose titrations of serum were incubated with the bacterial strain and specific IgG1- or IgG2b-binding visualized by FACS-analysis. Data were then normalized to the total amount of IgG1 or IgG2b present in serum (x-axis) as determined by ELISA. All curves represent individual mice from one of 2 independent experiments.

Fig. 4. Disturbance of host-microbial mutualism in human patients with liver dysfunction. (**A**) Serum IgG titers against the indicated bacteria in NAFLD patients (open symbols) compared to age- and sex-matched healthy controls (filled dots). Pure cultures of the indicated bacteria were stained with dose-titrations of serum from patients or controls. Serum antibody coating of bacteria was visualised using monoclonal DyLight-conjugated anti-human IgG and quantified per bacterium by flow cytometry. Resulting MFI was plotted against total IgG added to the assay as determined by ELISA and IgG-titers calculated by fitting 4-parameter logistic curves to each

donor and determining the concentration of IgG required to give a median fluorescence intensity binding of 80. The inverse of this IgG concentration is shown, for ease of interpretation. Each point represents an individual subject and lines show means. Unpaired t-test or one-way ANOVA and Tukey post-test were used to compare the groups; *, p≤0.05, **; p≤0.01. (**B**) Cluster-analysis from Basel NAFLD patients with different stages of liver disease (steatosis = blue, NASH = yellow, cirrhosis = red) and age- and sex-matched healthy controls (green). Heatmaps were generated using an euclidean distance function with complete linkage clustering in the statistical package R using the package "gplots version 2.8.0", function "heatmap.2". Red indicates increased and blue decreased titers compared to the mean of the entire population.

Supplementary Materials:

Figs. S1-S9

Supplementary Figure Legends:

Fig. S1. (A) Bacterial counts in peripheral and portal blood in 8-10 weeks old C57BL/6 mice at the indicated time-points after either oral gavage of 10^{10} or i.v. injection of 10^{7} live *E. coli.* Each data point represents a single animal from one experiment. The dashed line indicates the detection limit. **(B)** Vascular supply of the liver and the spleen. Both liver (brown) and spleen (red) receive arterial blood (red) from the abdominal aorta via the hepatic or splenic artery respectively. The portal vein (blue) collects venous blood from the mesentery and delivers it to the liver for filtration. Venous blood leaving the spleen (blue) drains into the portal vein as well. Liver sinusoids architecture is shown on the left side. Hepatocytes are lined with a fenestrated endothelium. Liver Kupffer cells placed within this network rapidly phagocytose potentially harmful products. Hepatic stellate cells located underneath the endothelial layer are important for liver repair.

Fig. S2. (A) Bacterial counts in peripheral blood (open circles) and spleen (filled dots) in 8-10 weeks old C57BL/6 mice after 3 weeks of DSS treatment. Each data point represents one mouse from one experiment. The dashed line indicates the detection limit. **(B)** Representative FACS plots after anti-F4/80 staining on collagenase-digested Percoll-purified liver mononuclear cells of control (left) and clodronate liposome injected mice. Shown are means ± SD of n=3 mice per group.

Fig. S3. (**A-C**) Bacterial counts in peripheral blood at the indicated time-points after intra-venous injection of 10^{7} live *E. coli* into the tail vein of CCl_4 treated (filled dots, solid lines) or olive-oil treated control mice (open circles, dashed lines) after 6, 12 or 16 weeks of treatment. Shown are

pooled data from one (C) or two (A, B) independent experiments. Joining lines connect the means of each group. The horizontal dashed line represents the detection-limit. (**D**) Bacterial counts in the liver of 16 weeks CCl_4 treated (black dots) or healthy control mice (open circles) 6 hours after live bacterial challenge with 10^7 *E. coli* into the tail vein. C57BL/6 mice were intra-peritoneally injected two times per week with CCl_4 or olive oil respectively for 6, 12 or 16 weeks respectively. Horizontal lines show means. Unpaired t-test was used to compare the groups.

Fig. S4. (**A, B**) Peripheral blood granulocytes and serum lipocalin 2 levels in sham-operated or BDL-treated mice before intra-venous challenge with live bacteria. Mice were analysed 3 weeks after surgery. Each point represents one individual mouse from two independent experiments and horizontal lines show means. Unpaired t-test was used to compare the groups.

Fig. S5. (**A**) Representative H&E stained liver sections of bile-duct ligated (BDL) or sham-operated 10-weeks old NMRI mice 3 weeks after surgery. (**B**) Representative H&E stained liver sections of CCl_4 treated or healthy control mice 6 or 12 weeks after treatment. **(C)** Representative Masson's Trichrome stained liver sections of CCl_4 treated or healthy control mice 6, 12 or 16 weeks after treatment. **(D)** Representative F4/80 stained liver sections of CCl_4 treated or healthy control mice at week 12. CCl_4 was dissolved in olive oil and administered intraperitoneally two times per week. Control mice received olive oil only. Note development of portal fibrosis and bile duct proliferation (arrows).

Fig. S6. (**A, B**) Bacterial counts in peripheral blood and liver 3 hours after injection of 10^7 live *E. coli* into the tail vein. All mice were treated 3 times per week with PBS alone or with 1 µg LPS from *Salmonella typhimurium* intraperitoneally and analysed 48h after the final treatment. All mice were then intravenously injected with 10^7 live *E. coli.* Bacterial counts were determined per 50 µl blood or organ. Each data point represents a single animal from one experiment and

horizontal lines show means. Unpaired t-test was used to compare the groups. (**C**) Bacterial counts in mesenteric lymph nodes or the thoracic duct lymph 6 hours after oral gavage with 10^{10} live *E. coli* JM83 in healthy control (open circles) or CCl_4 treated (filled dots) C57BL/6 mice. CCl_4 was dissolved in olive oil and administered intra-peritoneally two times per week over 6 weeks. Control mice received olive oil only. Each data point represents a single mouse from one experiment and horizontal lines show means. The dashed line indicates the detection limit. Unpaired t-test was used to compare the groups.

Fig. S7. (A) Representative H&E stained colons and small intestines of fibrotic (CCl_4) or healthy control mice. CCl_4 was dissolved in olive oil and administered intraperitoneally two times per week over 6 and 12 weeks respectively. Control mice received olive oil only. **(B)** H&E stained colons and small intestines of bile-duct ligated (BDL) or sham-operated 10-weeks old NMRI mice 3 weeks after surgery. Note development of oedema (asterisks), leukocyte infiltrate (arrows) and exudate (arrowheads) in BDL mice. (**C**) Faecal lipocalin 2 values in the same mice as in A as determined by ELISA. Each point represents one mouse from one experiment. The dashed line represents the detection-limit. Unpaired t-test was used to compare the groups.

Fig. S8. (A, B) Serum IgG titers of the mice and rats shown in Fig. 3 G and H. IgG-titers were calculated by fitting 4-parameter logistic curves to each sample and determining the concentration of IgG required to give a median fluorescence intensity binding above background staining. The inverse of this IgG concentration is shown, for ease of interpretation. Each data point represents one mouse from one experiment. Unpaired t-test was used to compare the groups.

Fig. S9. (**A**) IgA titers against the indicated bacteria in NAFLD patients (open symbols) compared to age- and sex-matched healthy controls (filled dots). Pure cultures of the indicated

bacteria were stained with dose-titrations of serum from patients or controls. Serum antibody coating of bacteria was visualised using monoclonal FITC-conjugated anti-human IgA and quantified per bacterium by flow cytometry. Resulting MFI was plotted against total IgA added to the assay as determined by ELISA and IgA-titers calculated by fitting 4-parameter logistic curves to each donor and determining the concentration of IgA required to give a median fluorescence intensity binding of 80. The inverse of this IgA concentration is shown, for ease of interpretation. Each point represents an individual subject and lines show means. Unpaired t-test or one-way ANOVA and Tukey post-test were used to compare the groups; *p≤0.05, **p≤0.01. (**B**) Cluster-analysis from Rome NAFLD patients (blue) and healthy controls (yellow) for 8 different anti-microbiota IgG and IgA titers. Heatmaps were generated using an euclidean distance function with complete linkage clustering in the statistical package R using the package "gplots version 2.8.0", function "heatmap.2". Red indicates increased and blue decreased titers compared to the mean of the entire population.

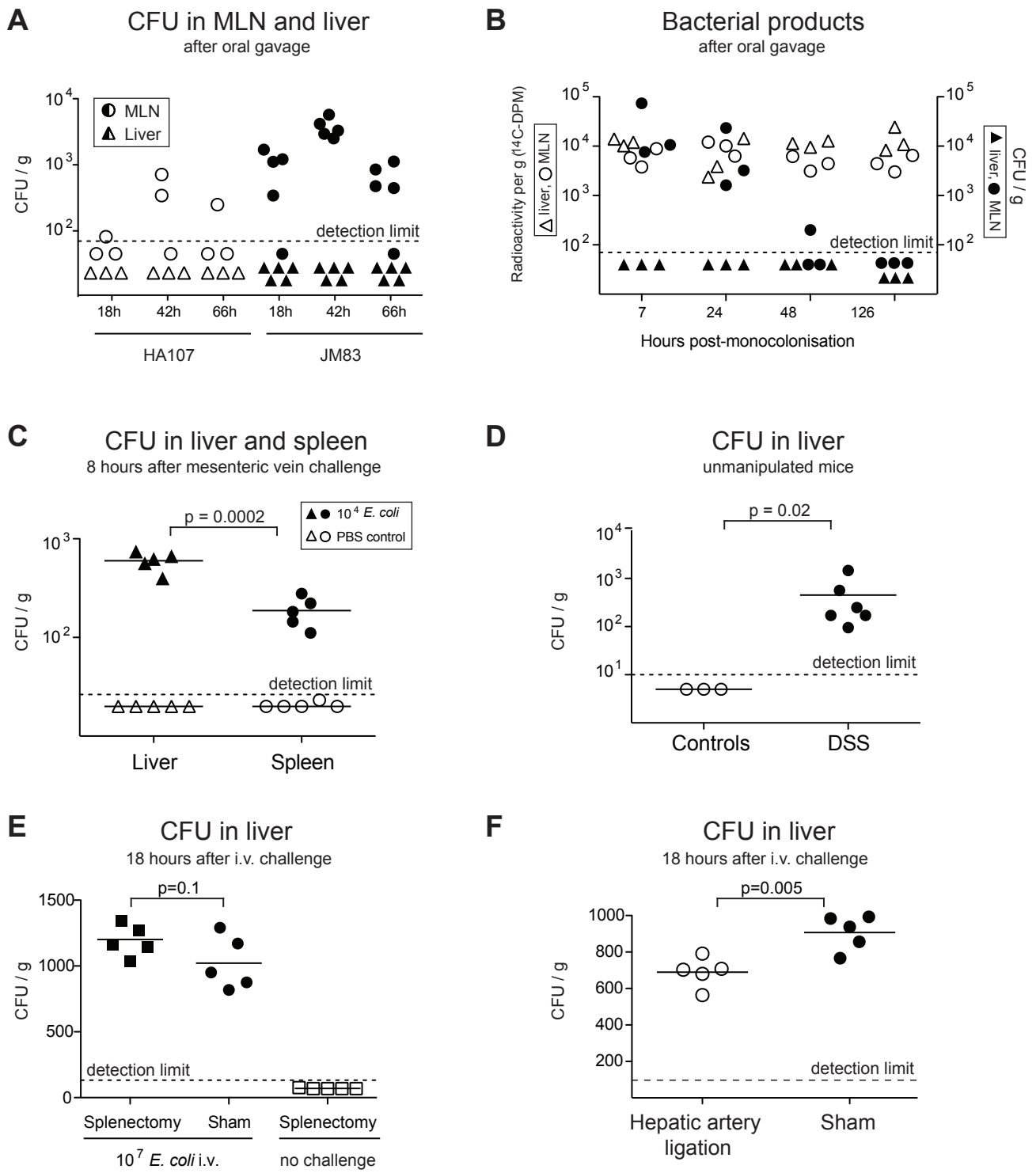

Balmer *et al.* Figure 1

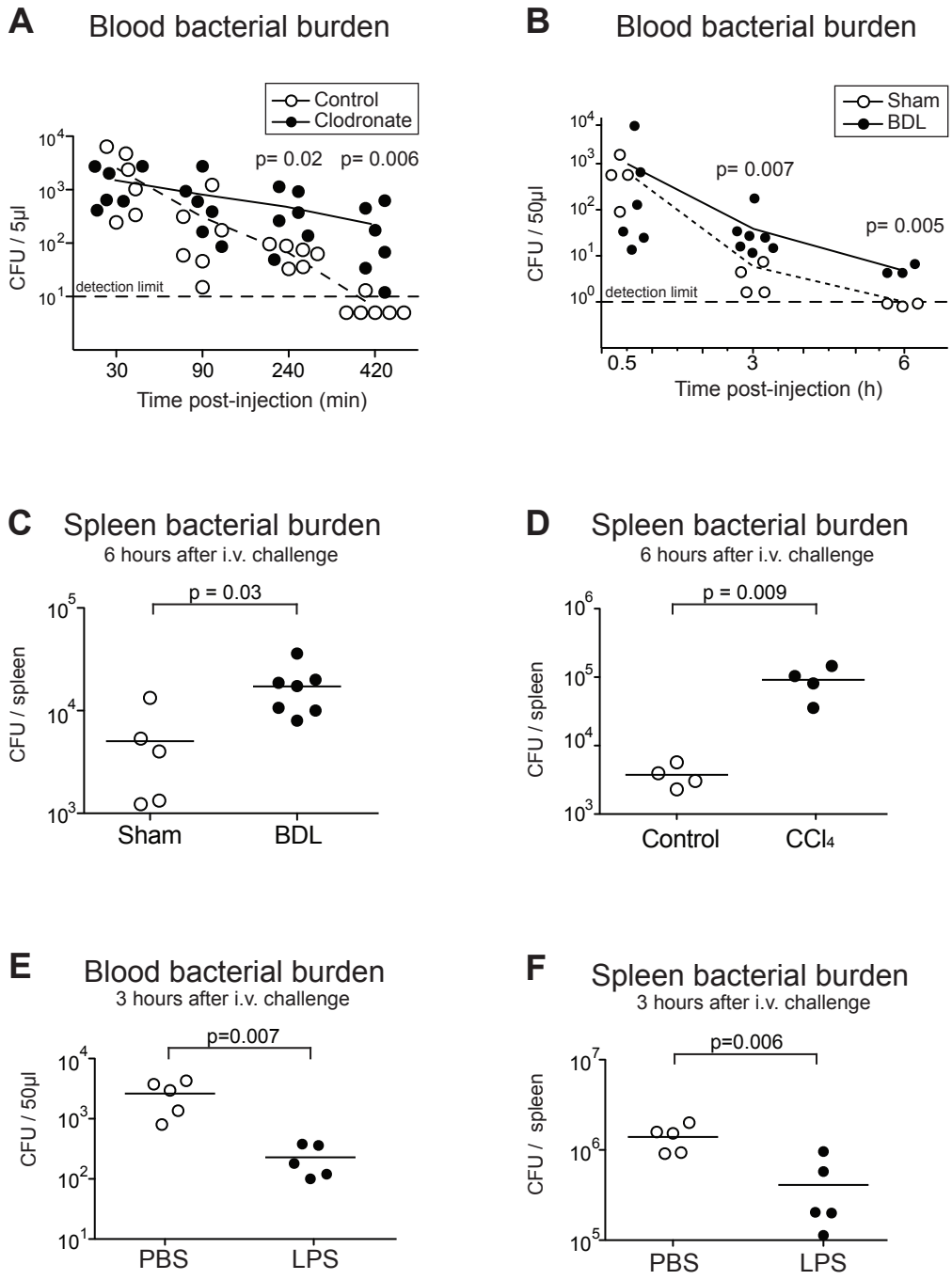

Balmer *et al.* Figure 2

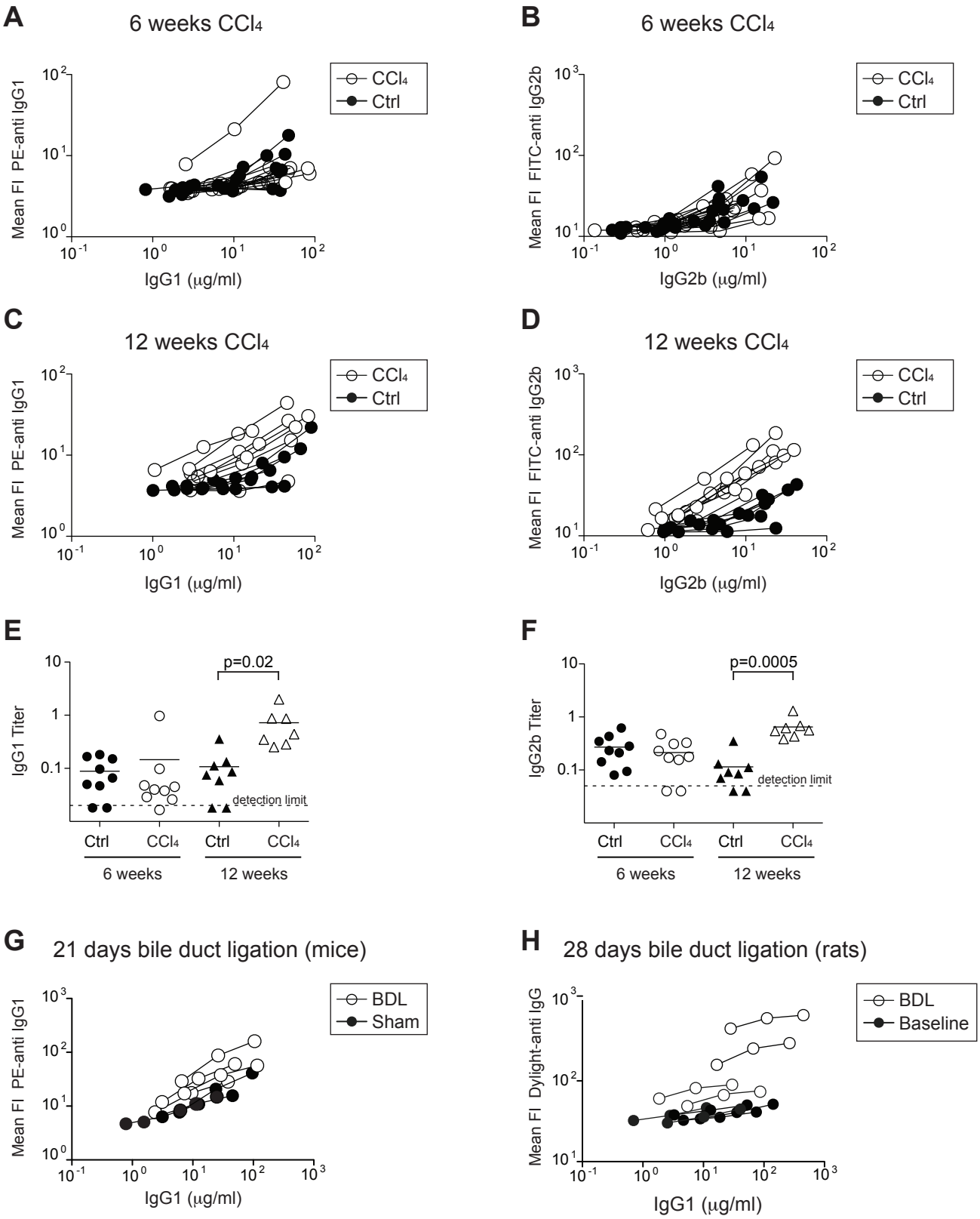

Balmer *et al*. Figure 3

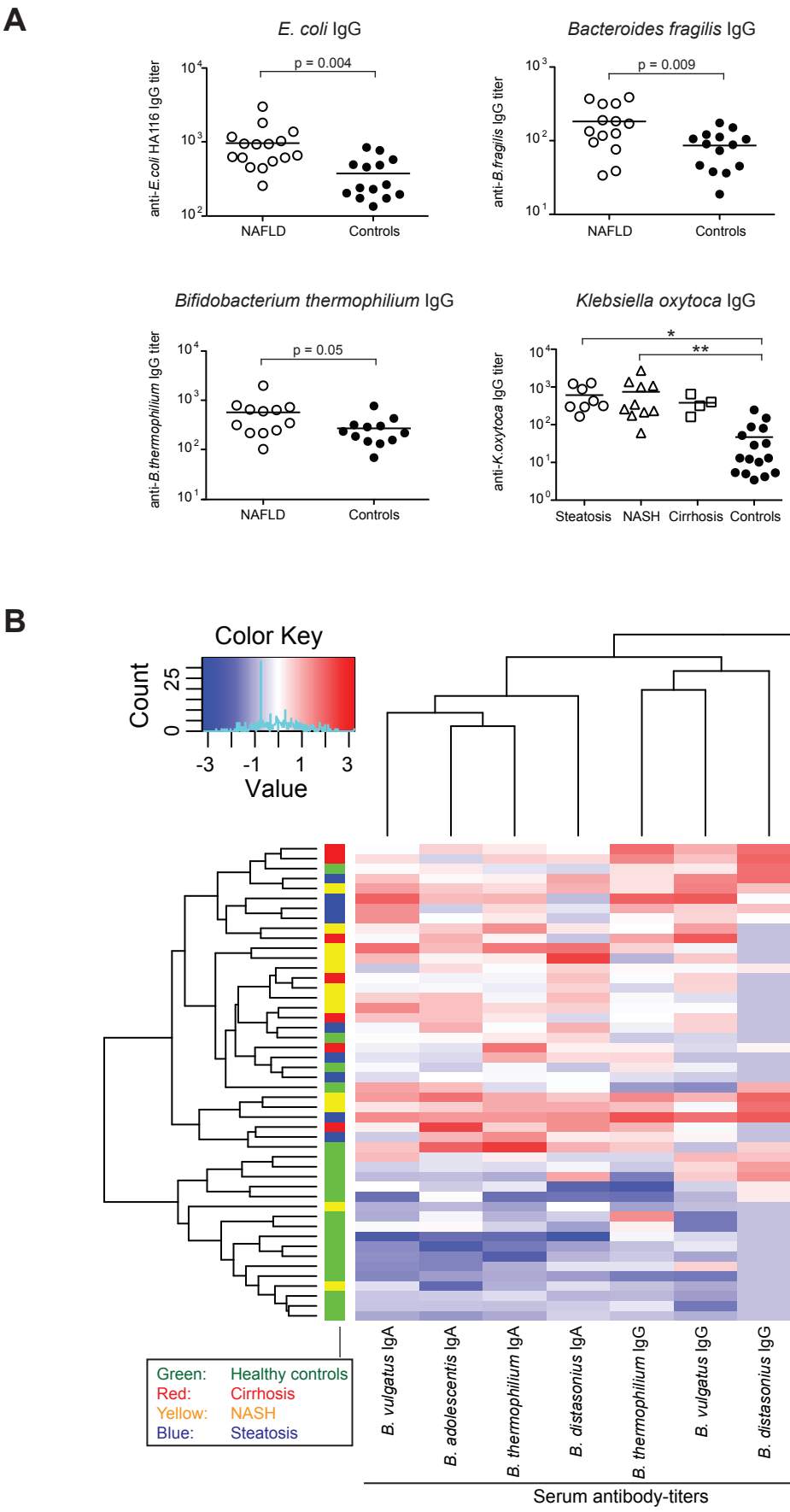

Balmer *et al.* Figure 4

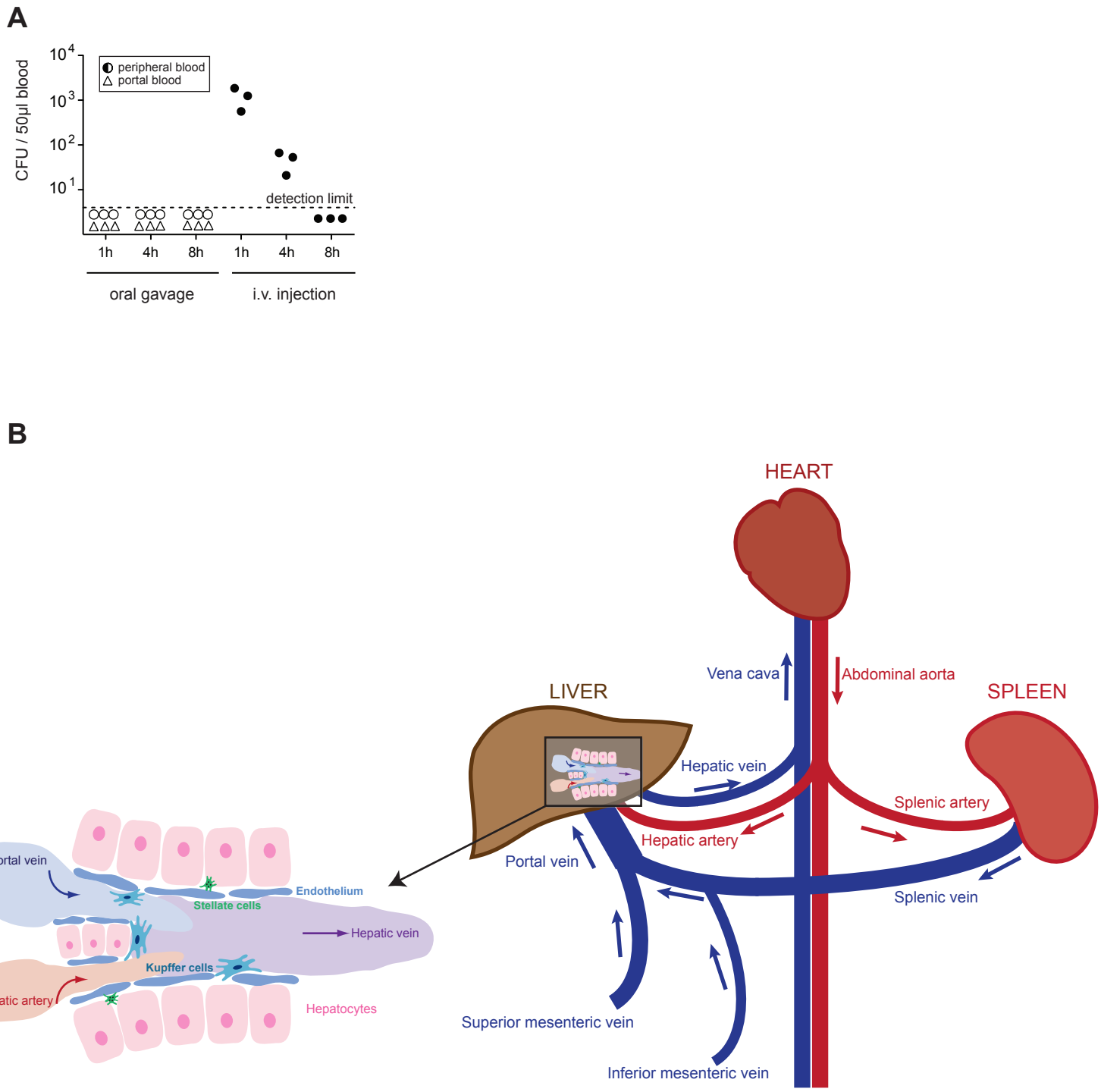

Balmer *et al.* Supplementary Figure 1

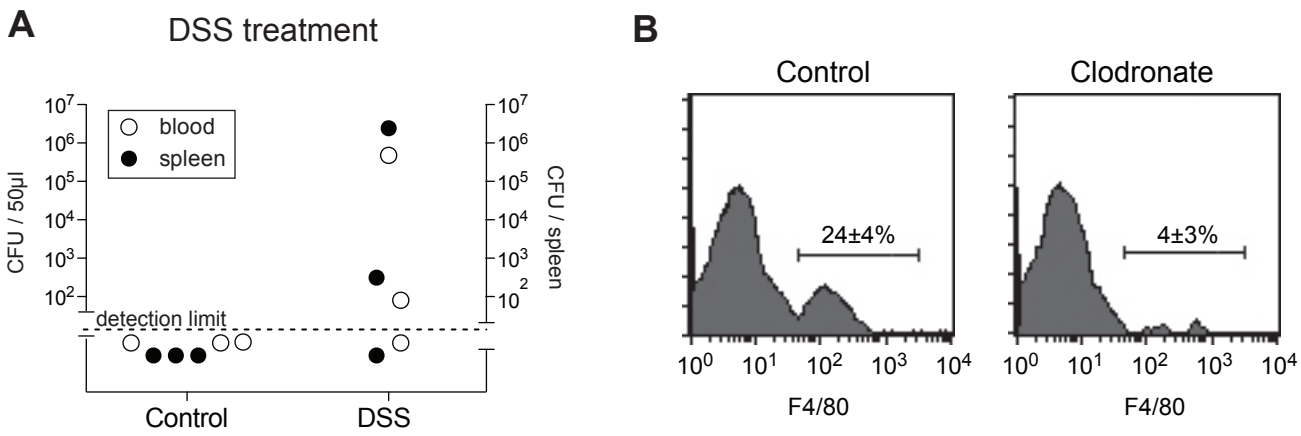

Balmer *et al.* Supplementary Figure 2

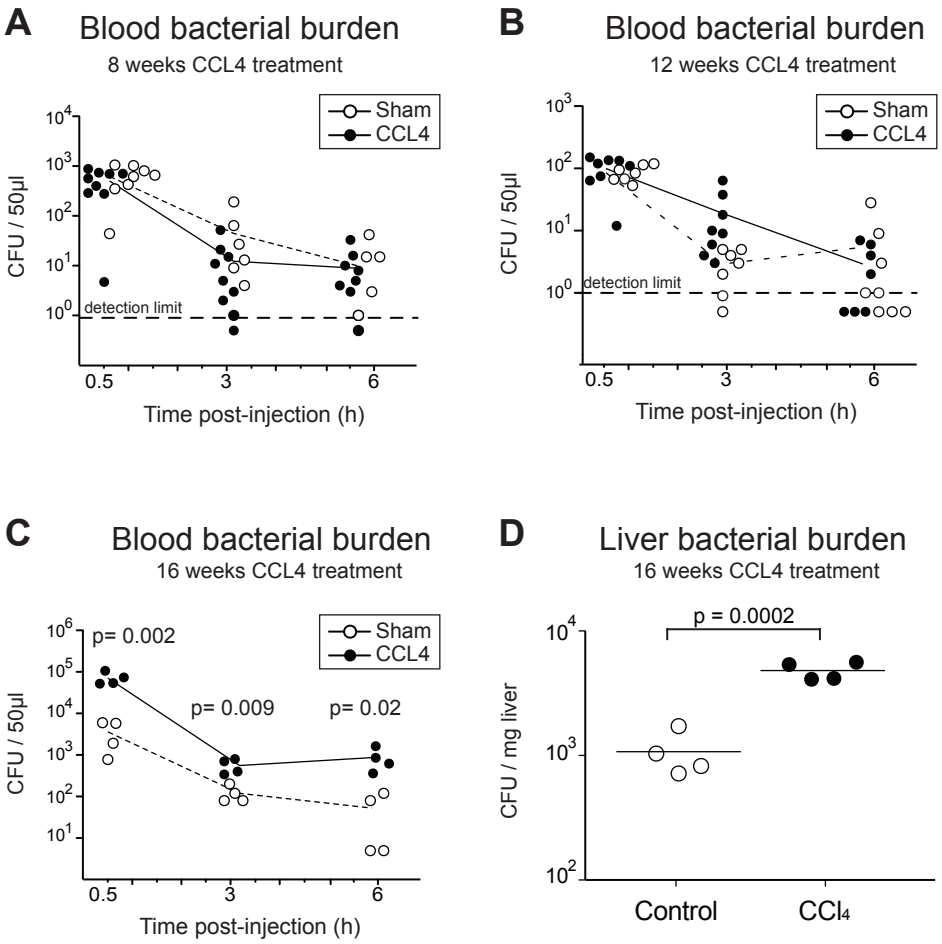

Balmer *et al.* Supplementary Figure 3

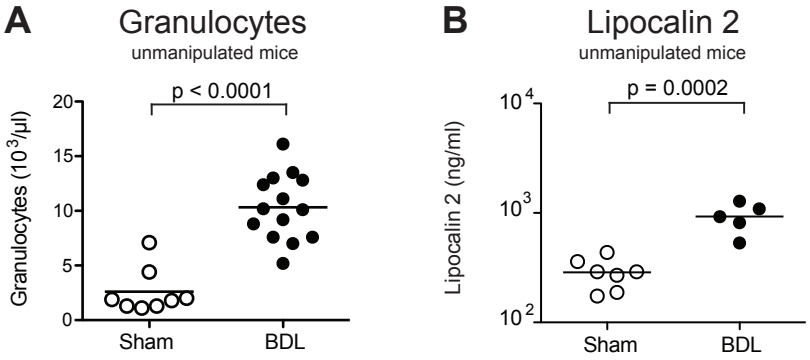

Balmer *et al.* Supplementary Figure 4

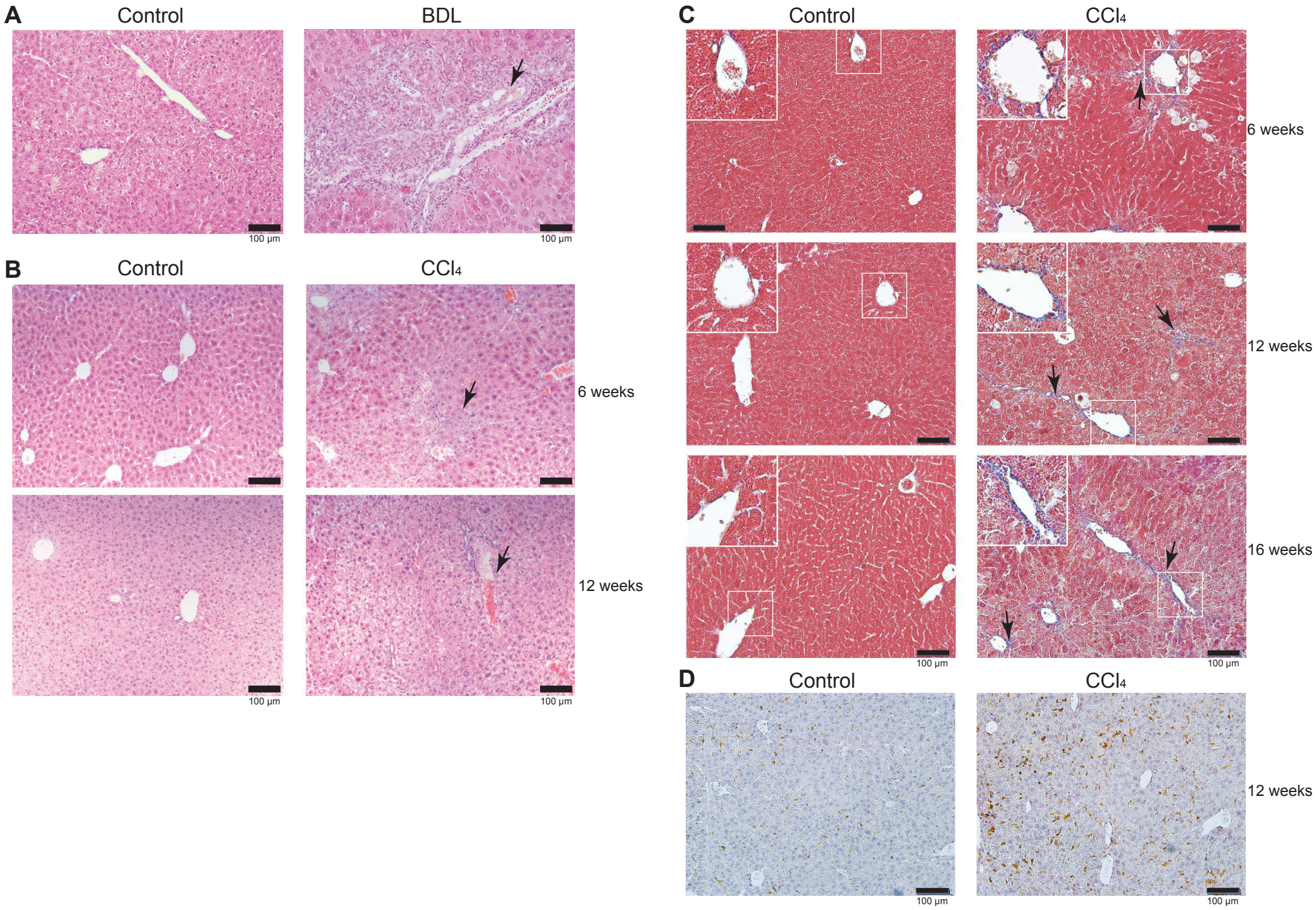

Balmer *et al.* Supplementary Figure 5

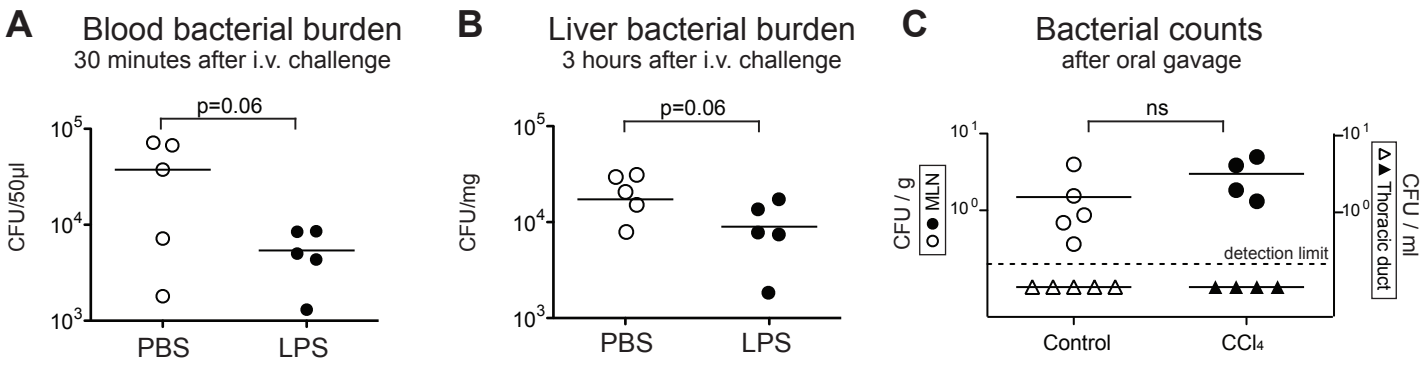

Balmer *et al.* Supplementary Figure 6

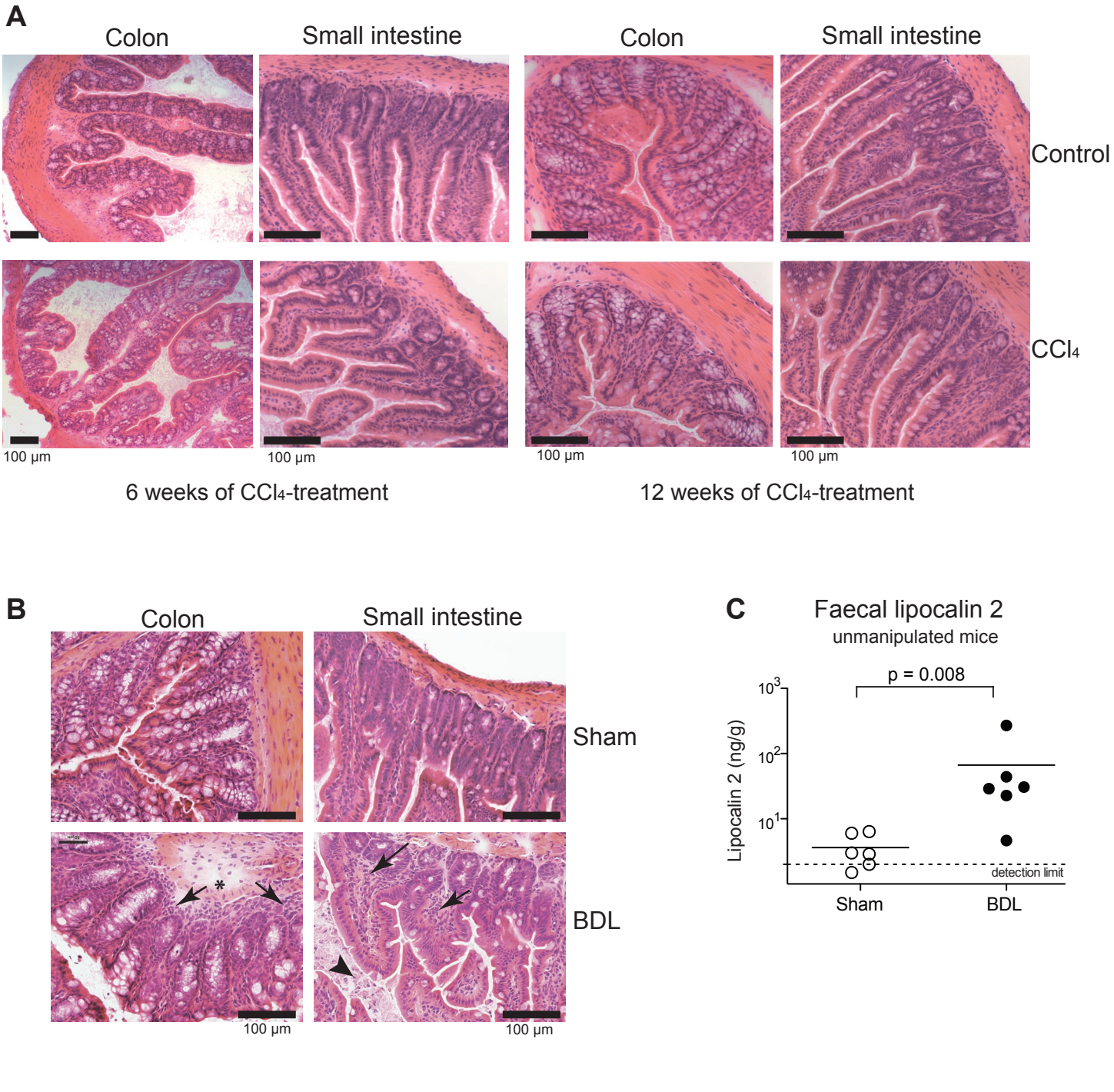

Balmer *et al.* Supplementary Figure 7

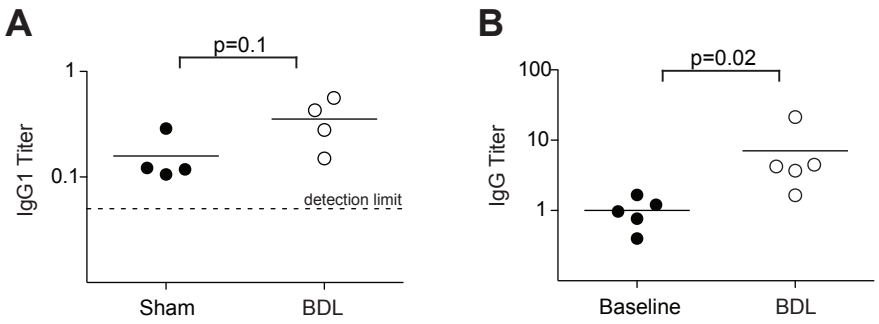

Balmer *et al*. Supplementary Figure 8

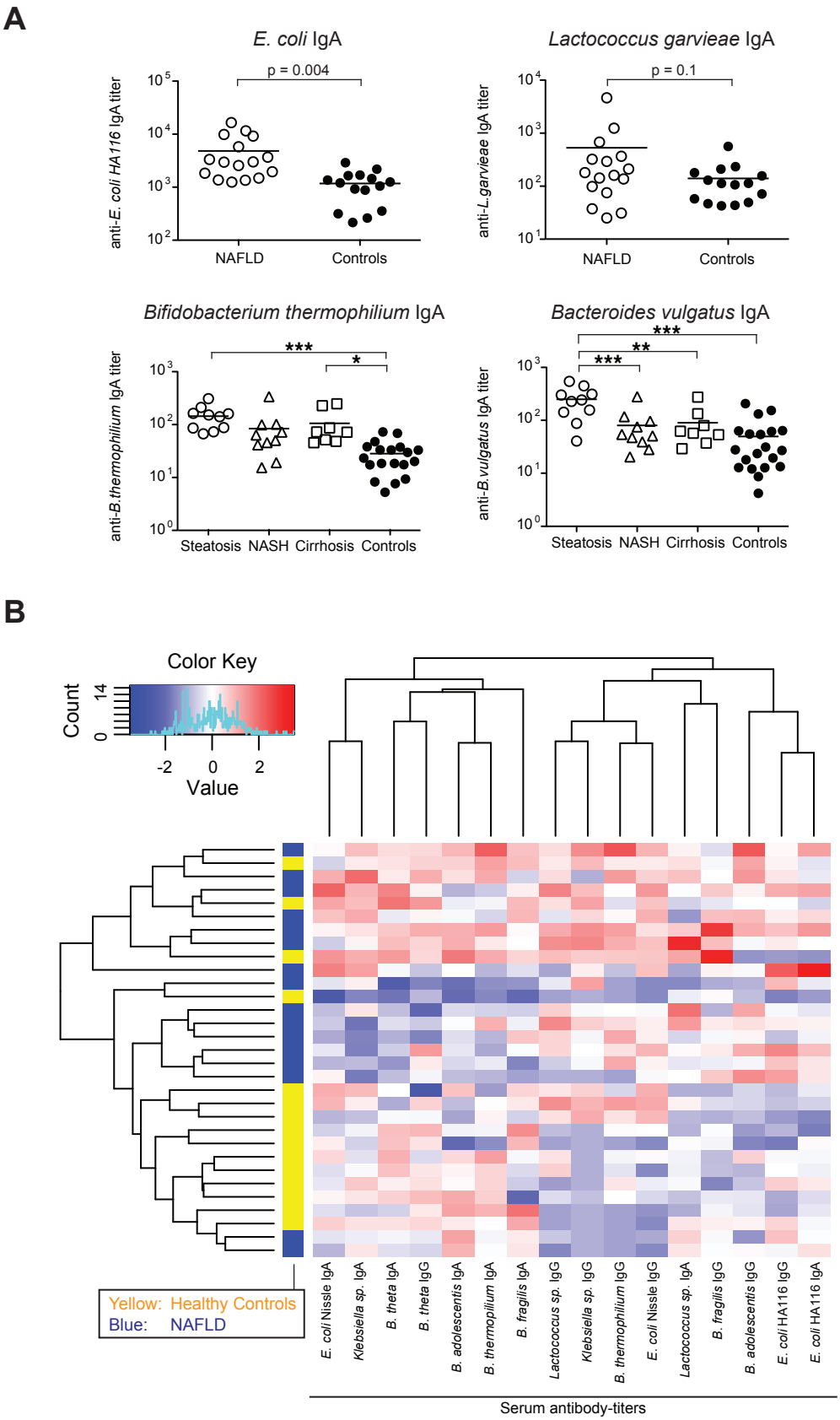

Balmer *et al.* Supplementary Figure 9